

Limits of open circuit voltage in organic photovoltaic devices

M. F. Lo, T. W. Ng, T. Z. Liu, V. A. L. Roy, S. L. Lai, M. K. Fung, C. S. Lee, and S. T. Lee

Citation: [Applied Physics Letters](#) **96**, 113303 (2010); doi: 10.1063/1.3360336

View online: <http://dx.doi.org/10.1063/1.3360336>

View Table of Contents: <http://scitation.aip.org/content/aip/journal/apl/96/11?ver=pdfcov>

Published by the [AIP Publishing](#)

Articles you may be interested in

[Fullerene acceptor for improving open-circuit voltage in inverted organic photovoltaic devices without accompanying decrease in short-circuit current density](#)

Appl. Phys. Lett. **100**, 063303 (2012); 10.1063/1.3683469

[Enhancement of the short circuit current in organic photovoltaic devices with microcavity structures](#)

Appl. Phys. Lett. **97**, 083306 (2010); 10.1063/1.3480612

[Operation of a reversed pentacene-fullerene discrete heterojunction photovoltaic device](#)

Appl. Phys. Lett. **90**, 113505 (2007); 10.1063/1.2713345

[High open circuit voltage organic photovoltaic cells based on oligothiophene derivatives](#)

Appl. Phys. Lett. **89**, 213501 (2006); 10.1063/1.2392823

[Molecular level control of donor/acceptor heterostructures in organic photovoltaic devices](#)

Appl. Phys. Lett. **85**, 663 (2004); 10.1063/1.1775891



Limits of open circuit voltage in organic photovoltaic devices

M. F. Lo, T. W. Ng, T. Z. Liu, V. A. L. Roy, S. L. Lai, M. K. Fung, C. S. Lee,^{a)} and S. T. Lee

Department of Physics and Materials Science, Center of Super-Diamond and Advanced Films (COSDAF), City University of Hong Kong, Hong Kong Special Administrative Region, People's Republic of China

(Received 19 January 2010; accepted 17 February 2010; published online 18 March 2010)

Open circuit voltage (V_{oc}) of organic photovoltaic devices has been interpreted with either the metal-insulator-metal (MIM) model or the energy offset between highest occupied molecular orbital (HOMO) of the donor and the lowest unoccupied molecular orbital (LUMO) of the acceptor ($HOMO_D-LUMO_A$). To elucidate the relation between V_{oc} and the two models, we have used electrodes of a wide range of work functions to connect the CuPc/C₆₀ organic photovoltaic devices. We found that when the work function difference ($\Delta\phi_{electrodes}$) between ITO and Al electrode is in the range -3 and 0 eV, V_{oc} increases linearly with $\Delta\phi_{electrodes}$ as prescribed by the MIM model. Outside this range, V_{oc} saturates with values close to that given by the $HOMO_D-LUMO_A$ less the exciton binding energy. © 2010 American Institute of Physics. [doi:10.1063/1.3360336]

Organic photovoltaic (OPV) devices have received much attention recently for potential applications as low-cost renewable energy devices.^{1,2} While recent progress in OPV performance is encouraging, OPV device efficiency is still below commercial requirements.²⁻⁴ As the open circuit voltage (V_{oc}) of OPV device is one important factor controlling the efficiency, it is essential to understand the physical origins and possible methods for increasing the V_{oc} .

Early OPV studies have shown that V_{oc} depends linearly on the work function difference ($\Delta\phi_{electrodes}$) between the two electrodes, as described by metal-insulator-metal (MIM) model.^{5,6} By using Ca, Ag, Al, and Au as cathodes and ITO as anode, a linear relationship between the V_{oc} and metal work function with a slope parameter (S) ~ 0.1 was observed.⁵ The small slope parameter ($S \sim 0.1$) is attributed to Fermi level pinning at the organic/metal interface.^{5,7} Charge transfer at the organic/metal interface is suggested to reduce the slope parameter and thus the V_{oc} .^{6,7} On the other hand, Scharber *et al.*⁸ have later shown that the V_{oc} changes linearly with the energy level offset between the highest occupied molecular orbital (HOMO) of the donor and the lowest unoccupied molecular orbital (LUMO) of the acceptor ($HOMO_D-LUMO_A$). Recently, Rand *et al.*⁹ have shown that the $HOMO_D-LUMO_A$ offset limits the maximum possible V_{oc} in OPV devices. Different studies have been carried out aiming to control the $HOMO_D-LUMO_A$ offset by employing a donor material (D) with a deeper HOMO level and/or

an acceptor material (A) with a more shallow HOMO level.^{7,8,10-12} In short, both the MIM model and the $HOMO_D-LUMO_A$ offset model have their respective experimental supports. So far no consistent picture has been proposed to reconcile the gap between the two models.

In this work, we use a range of electrodes and buffer layers to vary the work function difference between the two electrodes from -4.0 to $+2.4$ V in a typical copper phthalocyanine/fullerene (CuPc/C₆₀) cell. We observe that the V_{oc} changes linearly with $\Delta\phi_{electrodes}$, when the magnitude of $\Delta\phi_{electrodes}$ is in the range of -3 – 0 V (i.e., follows the MIM model). Outside this range, the V_{oc} saturates and shows little change to further $\Delta\phi_{electrodes}$ changes. These results suggest that the changes in V_{oc} can be consistently considered within a coherent picture incorporating the MIM and the $HOMO_D-LUMO_A$ offset models. It is shown that the $HOMO_D-LUMO_A$ offset set a limit on the maximum possible V_{oc} as reported by Rand *et al.*⁹ Meanwhile, V_{oc} is linearly dependent on the $\Delta\phi_{electrodes}$ provided that it is smaller than $HOMO_D-LUMO_A$ energy offset after subtracting the exciton binding energy (E_B).

Patterned indium-tin-oxide (ITO) coated glass substrates with a sheet resistance of $30 \Omega/\text{square}$ were first cleaned with Decon 90, rinsed in deionized water, dried in an oven, and finally treated in an ultraviolet-ozone chamber. A series of devices were fabricated by using CuPc and C₆₀, respectively, as the donor and the acceptor materials. Bathocu-

TABLE I. Key photovoltaic responses for type A devices with different buffer layer.

Devices with conventional structure	ϕ_{bottom}/eV	ϕ_{top}/eV	$\Delta\phi_{electrode}/\text{eV}$	V_{oc}/V	$J_{sc}/\text{mA}/\text{cm}^2$
ITO/CsF(0 nm)/CuPc/C ₆₀ /BcP/Al	5.0	4.2	0.8	0.46	-6.4
ITO/CsF(0.2 nm)/CuPc/C ₆₀ /BcP/Al	4.2	4.2	0.0	0.42	-3.6
ITO/CsF(0.5 nm)/CuPc/C ₆₀ /BcP/Al	3.9	4.2	-0.3	0.34	-3.3
ITO/CsF(1.0 nm)/CuPc/C ₆₀ /BcP/Al	3.6	4.2	-0.6	0.25	-2.5
ITO/CsF(0 nm)/CuPc/C ₆₀ /BcP/Yb	5.0	2.6	2.4	0.46	-4.7

^{a)} Author to whom correspondence should be addressed. Electronic mail: apcslee@cityu.edu.hk.

TABLE II. Key photovoltaic responses for type B devices with different buffer layer.

Devices with inverted structure	$\phi_{\text{bottom}}/\text{eV}$	$\phi_{\text{top}}/\text{eV}$	$\Delta\phi_{\text{electrode}}/\text{eV}$	V_{oc}/V	$J_{\text{sc}}/\text{mA}/\text{cm}^2$
ITO/CsF(0.5 nm)/C ₆₀ /CuPc/MoO ₃ (1.5 nm)/Al	3.9	5.5	-1.6	0	0
ITO/CsF(0.5 nm)/C ₆₀ /CuPc/MoO ₃ (5 nm)/Al	3.9	6.6	-2.7	-0.26	1.3
ITO/CsF(0.5 nm)/C ₆₀ /CuPc/MoO ₃ (7.5 nm)/Al	3.9	6.8	-2.9	-0.31	1.8
ITO/CsF(0 nm)/C ₆₀ /CuPc/MoO ₃ (7.5 nm)/Al	5.0	6.8	-1.8	-0.098	1.5
ITO/CsF(1.5 nm)/C ₆₀ /CuPc/MoO ₃ (7.5 nm)/Al	3.3	6.8	-3.5	-0.33	2.5
ITO/CsF(3 nm)/C ₆₀ /CuPc/MoO ₃ (10 nm)/Al	3.0	6.9	-3.9	-0.40	2.9
ITO/CsF(4 nm)/C ₆₀ /CuPc/MoO ₃ (10 nm)/Al	2.9	6.9	-4.0	-0.40	4.5

proline and molybdenum oxide (MoO₃) were used to prevent exciton quenching while providing electron and hole conduction to the Al electrode.¹³ Cesium fluoride (CsF) and MoO₃ were used as buffer layers to modify the work function of the electrodes. Two types of devices were fabricated with the configurations of: ITO/CsF(*x* nm)/CuPc(34 nm)/C₆₀(44 nm)/BcP(5 nm)/Al(80 nm) or Yb(80 nm) (conventional devices) and ITO/CsF(*x* nm)/C₆₀(44 nm)/CuPc(34 nm)/MoO₃(*x* nm)/Al(80 nm) (inverted devices). Detailed device structures are summarized in Table I and II. Following deposition of organic molecules, Al or Yb cathode (80 nm) was deposited by thermal evaporation using a shadow mask to define an active device area of 0.1 cm². All organic materials CuPc (Luminescence Technology Corp.: sublimated twice), C₆₀ (ADS 99.95%), BCP (Acros 98%), MoO₃ (Luminescence Technology Corp.) and CsF (Aldrich 99%) were used as received without further purification. The deposition rates were monitored using a quartz oscillating crystal and was controlled at 0.1–0.2 nm/s for both organic and metal layers. Current-voltage (I-V) characteristics of OPV devices were measured with a programmable Keithley model 237 power source. Photocurrent was measured in the dark and under illumination with an intensity of 100 mW/cm² from an Oriel 150 W solar simulator with AM1.5G (AM: air mass, G: global) filters. The light intensity was calibrated with an Oriel radiant power meter.¹² Effective work functions of the two electrodes were measured by ultraviolet photoemission spectrometry.¹⁴

Figure 1 shows the variation of the work function of the ITO substrate after deposition of (a) MoO₃ and (b) CsF buffer layers. The work function increases (decreases) as the thickness of MoO₃ (CsF) increases. By changing the buffer layer thickness the work function can be continuously tuned

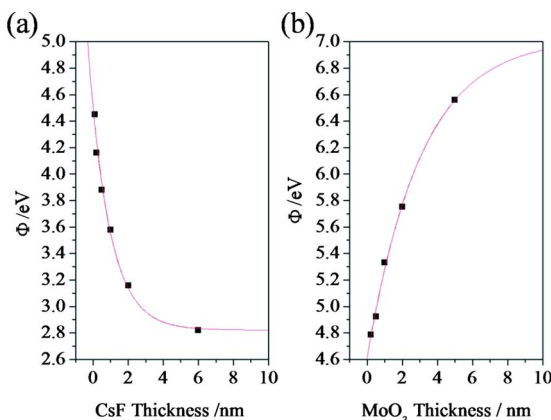


FIG. 1. (Color online) Work function of (a) MoO₃ (b) CsF buffer layer of different thickness on ITO.

from 2.8 eV (6 nm of CsF) to 6.6 eV (5 nm of MoO₃). Together with an Al or Yb electrode and inversion of the CuPc/C₆₀ layers, a wide range of $\Delta\phi_{\text{electrodes}}$ from -4.0 to +2.4 V can be achieved as tabulated in Table I together with the corresponding V_{oc} and J_{sc} .

As shown in Table I, the conventional type A devices show a negative J_{sc} and a positive V_{oc} providing photovoltaic output power in the fourth quadrant of the I-V curve. In contrast, the output powers for type B devices are located at the second quadrant of the I-V curve. Thus, upon solar illumination, hole and electron would respectively flow out of the Al and the ITO electrodes. The polarity switch from type A to type B devices is attributed to the reverse in potential gradient developed by $\Delta\phi_{\text{electrodes}}$.

Figure 2 shows the relation between V_{oc} and $\Delta\phi_{\text{electrodes}}$ of the devices. It can be seen that V_{oc} of both types of devices increases linearly with $\Delta\phi_{\text{electrodes}}$ when $\Delta\phi_{\text{electrodes}}$ is between -3 and 0 eV, revealing that the relation of V_{oc} with $\Delta\phi_{\text{electrodes}}$ can be well described by the MIM model in region II. Since V_{oc} can be influenced by $\Delta\phi_{\text{electrode}}$, it is important to study the variation of $\Delta\phi_{\text{electrode}}$ over a wide range. Interestingly, Fig. 2 shows that V_{oc} approaches a saturated value of ~0.46 and -0.40 V when $\Delta\phi_{\text{electrode}}$ is outside of region II. Significantly, the saturation values are close to the value given by $V_{\text{oc}} = \text{HOMO}_{\text{D}} - \text{LUMO}_{\text{A}} - E_{\text{B}}$.^{9,15}

The maxima of the measured V_{oc} in the present CuPc/C₆₀ system are ~0.46 and -0.40 V, as denoted by the horizontal dashed lines in Fig. 2. From literature data^{4,16} the value of $\text{HOMO}_{\text{CuPc}} - \text{LUMO}_{\text{C60}}$ offset is estimated to be ~0.7 eV, which is denoted by the horizontal solid lines in Fig. 2. The larger energy difference between the solid and dashed line observed in the inverted device can be due to the

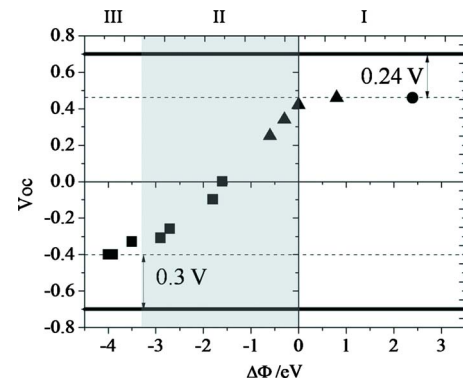


FIG. 2. (Color online) Measured V_{oc} against the work function differences between electrodes [\blacktriangle : ITO/CsF(*x* nm)/CuPc/C₆₀/BcP/Al, \bullet : ITO/CuPc/C₆₀/BcP/Yb, and \blacksquare : ITO/CsF(*x* nm)/CuPc/C₆₀/MoO₃(*x* nm)/Al]. The horizontal dashed lines indicate the saturated V_{oc} . The thick solid lines indicate the theoretical V_{oc} .

following reasons; (1) Fermi level pinning between ITO/CsF and C₆₀ in the inverted device. The charge transfer between metal/organic interface can also reduce the measured V_{oc} .^{6,7} (2) Reverse order of D and A materials un-favor the charge transport and injection across the ITO/CsF/C₆₀ and CuPc/MoO₃/Al interfaces. The reversed potential gradient at A and D materials probably reduces the V_{oc} .^{7,14} (3) The estimated theoretical V_{oc} depends on the value of E_B , where the E_B are different in CuPc and C₆₀. Thus, the location of exciton dissociation in either CuPc or C₆₀ would result in different theoretical V_{oc} .^{9,12} Consequently, V_{oc} would not be a fingerprint that is simply determined by the MIM model or the HOMO_D-LUMO_A offset alone. Rather, Rand's model provides the maximum possible V_{oc} , which is controlled by the HOMO_D-LUMO_A offset and E_B , whereas within the maxima V_{oc} depends linearly on $\Delta\phi_{\text{electrode}}$ following the MIM model.

In summary, we fabricated CuPc/C₆₀ OPV devices with electrodes having a wide range of work function differences ($\Delta\phi_{\text{electrode}}$ from -4.0 to $+2.4$ eV) by using different electrodes and buffer layers. Measurements of the OPV devices showed that when $\Delta\phi_{\text{electrode}}$ is in the range of -3 and 0 eV, V_{oc} increases linearly with $\Delta\phi_{\text{electrode}}$ as prescribed by the MIM model. Once outside this range V_{oc} is saturated at about 0.4 – 0.5 V. The results suggest that V_{oc} can thus be consistently described by a combined MIM-HOMO_D-LUMO_A offset model. That is, the maximum possible V_{oc} is determined by the HOMO_D-LUMO_A offset less the exciton binding energy, and within its maximum the

V_{oc} varies linearly with the work function differences of the electrodes.

This project was supported by the Research Grant Council of Hong Kong (Grant No. CityU 101707).

¹C. W. Tang, *Appl. Phys. Lett.* **48**, 183 (1986).

²P. Peumans and S. R. Forrest, *Appl. Phys. Lett.* **79**, 126 (2001).

³J. Drechsel, B. Männig, F. Kozlowshi, M. Pfeiffer, K. Leo, and H. Hoppe, *Appl. Phys. Lett.* **86**, 244102 (2005).

⁴M. Y. Chan, S. L. Lai, M. K. Fung, C. S. Lee, and S. T. Lee, *Appl. Phys. Lett.* **90**, 023504 (2007).

⁵V. D. Mihailetschi, P. W. M. Blom, J. C. Hummelen, and M. T. Rispens, *J. Appl. Phys.* **94**, 6849 (2003).

⁶C. J. Brabec, *Sol. Energy Mater. Sol. Cells* **83**, 273 (2004).

⁷C. J. Brabec, A. Cravino, D. Meissner, N. S. Sariciftci, T. Fromherz, M. T. Rispens, L. Sanchez, and J. C. Hummelen, *Adv. Funct. Mater.* **11**, 374 (2001).

⁸M. C. Scharber, D. Mühlbacher, M. Koppe, P. Denk, C. Waldauf, A. J. Heeger, and C. J. Brabec, *Adv. Mater. (Weinheim, Ger.)* **18**, 789 (2006).

⁹B. P. Rand, D. P. Burk, and S. R. Forrest, *Phys. Rev. B* **75**, 115327 (2007).

¹⁰K. L. Mutolo, E. I. Mayo, B. P. Rand, S. R. Forrest, and M. E. Thompson, *J. Am. Chem. Soc.* **128**, 8108 (2006).

¹¹Z. T. Liu, M. F. Lo, H. B. Wang, T. W. Ng, V. A. L. Roy, C. S. Lee, and S. T. Lee, *Appl. Phys. Lett.* **95**, 093307 (2009).

¹²S. L. Lai, M. F. Lo, M. Y. Chan, C. S. Lee, and S. T. Lee, *Appl. Phys. Lett.* **95**, 153303 (2009).

¹³D. W. Zhao, X. W. Sun, C. Y. Jiang, A. K. K. Kyaw, G. Q. Lo, and D. L. Kwong, *Appl. Phys. Lett.* **93**, 083305 (2008).

¹⁴T. W. Ng, M. F. Lo, Z. T. Liu, F. L. Wong, S. L. Lai, M. K. Fung, C. S. Lee, and S. T. Lee, *J. Appl. Phys.* **106**, 114501 (2009).

¹⁵P. Peumans and S. R. Forrest, *Chem. Phys. Lett.* **27**, 398 (2004).

¹⁶J. X. Tang, Y. C. Zhou, Z. T. Liu, C. S. Lee, and S. T. Lee, *Appl. Phys. Lett.* **93**, 043512 (2008).